nature cell biology

Asymmetrically inherited multidrug resistance transporters are recessive determinants in cellular replicative ageing

Amr Eldakak[1], Giulia Rancati[1], Boris Rubinstein[1], Parama Paul[1], Veronica Conaway[1] and Rong Li[1,2,3]

Cellular ageing is known to correlate with the accumulation of many harmful agents[1], but it is unclear whether ageing can also result from the deterioration of components that are beneficial to the cell, but have a low rate of renewal. Here, we report a group of plasma membrane-associated transporters in yeast, belonging to the multidrug resistance (MDR) protein families, that may represent the latter type of ageing determinants. During the division of a yeast cell, newly synthesized transporter proteins are deposited mostly into the growing bud, whereas previously synthesized MDR proteins remain tightly associated with the mother cortex. Thus, the new and old pools of membrane-bound MDR proteins are spatially segregated during yeast asymmetric cell division, with the older pool stably inherited by the ageing mother. A model based on the observed dynamics of MDR protein inheritance and turnover predicted a decline in MDR activity as the mother cell advances in replicative age. As MDR proteins have crucial roles in cellular metabolism, detoxification and stress response, their collective decline may lead to fitness loss at an advanced age. Supporting this hypothesis, mutants lacking certain MDR genes exhibited a reduced replicative lifespan (RLS), whereas introduction of only one extra copy of these MDR genes extended RLS.

The mechanism of asymmetric cell division allows unequal distribution of ageing factors to progeny cells, and leads to a 'youthful' and genetically stable population[2]. Budding yeast (*Saccharomyces cerevisiae*) cells have a finite RLS of 20–30 divisions, and each division gives rise to a 'new-born' bud with a reset RLS from a mother cell of varying replicative age[3]. This asymmetry in age during yeast cell divisions has been mainly attributed to the accumulation and asymmetric inheritance of extrachromosomal rDNA circles (ERC) and oxidatively damaged proteins in mother cells, whereas the buds are free of these deleterious materials[1,4,5]. However, it has been unclear whether there are recessive ageing factors; beneficial components that could become limiting as mother cells advance in replicative age.

Yeast cells make their buds through polarized growth, during which membrane and organelle materials are trafficked towards the nascent bud along oriented actin tracks[6]. A comprehensive survey of the green fluorescent protein (GFP)-tagged yeast protein-localization database[7] led us to identify a group of plasma membrane proteins (Supplementary Information, Table S1) that all belong to the MDR protein families[8]. During growth, these proteins exhibit a localization pattern opposite to the direction of polarized trafficking, as they concentrate in the mother cell cortex instead of the small, developing bud (Fig. 1a, b). Using a spindle marker (GFP–Tub1), we established that the distribution of these proteins was strongly biased towards the mother before the onset of anaphase; however, during anaphase their fluorescence increased in the bud, diminishing the asymmetry (Fig. 1c). Time-lapse microscopy of cells expressing, from the native genomic locus, GFP-tagged Tpo1 (a polyamine transporter[9] and utilised here as a representative of the MDR transporter group) showed that the rapid accumulation of Tpo1–GFP in the bud during anaphase was probably because of new protein deposition, as the fluorescence of the mother cell did not decrease (Fig. 1d). Although there was no decrease in the fluorescence of the mother cell, Tpo1–GFP deposition during anaphase was strongly biased: fluorescence increase in the mother cell was only 17% of that in the bud (Fig. 1e) . The appearance of Tpo1 in the bud requires activation of the anaphase-promoting complex, as the localization asymmetry was maintained in cells arrested in metaphase by treatment with nocodazole, or by maintaining cells carrying the temperature-sensitive *cdc23-1* mutation at 37 °C[10] (Fig. 1f, g). This also indicates that the lack of Tpo1–GFP in the bud was not because of a delay in GFP maturation after synthesis. Neither were the observed localization patterns an artefact of the carboxy-terminal tag, as the same observation was made with a GFP tag at the amino terminus of Tpo1 (Supplementary Information, Fig. S1a).

Microarray data available from the yeast genome database suggest that the majority of the MDR transporters show peak mRNA levels in

[1]Stowers Institute for Medical Research, 1000 East 50th Street, Kansas City, MO 64110, USA. [2]Department of Molecular and Integrative Physiology, University of Kansas Medical Center, 3901 Rainbow Boulevard, Kansas City, KS 66160, USA.
[3]Correspondence should be addressed to R.L. (e-mail: rli@stowers.org)

Received 25 May 2010; accepted 22 June 2010; published online 25 July 2010; DOI: 10.1038/ncb2085

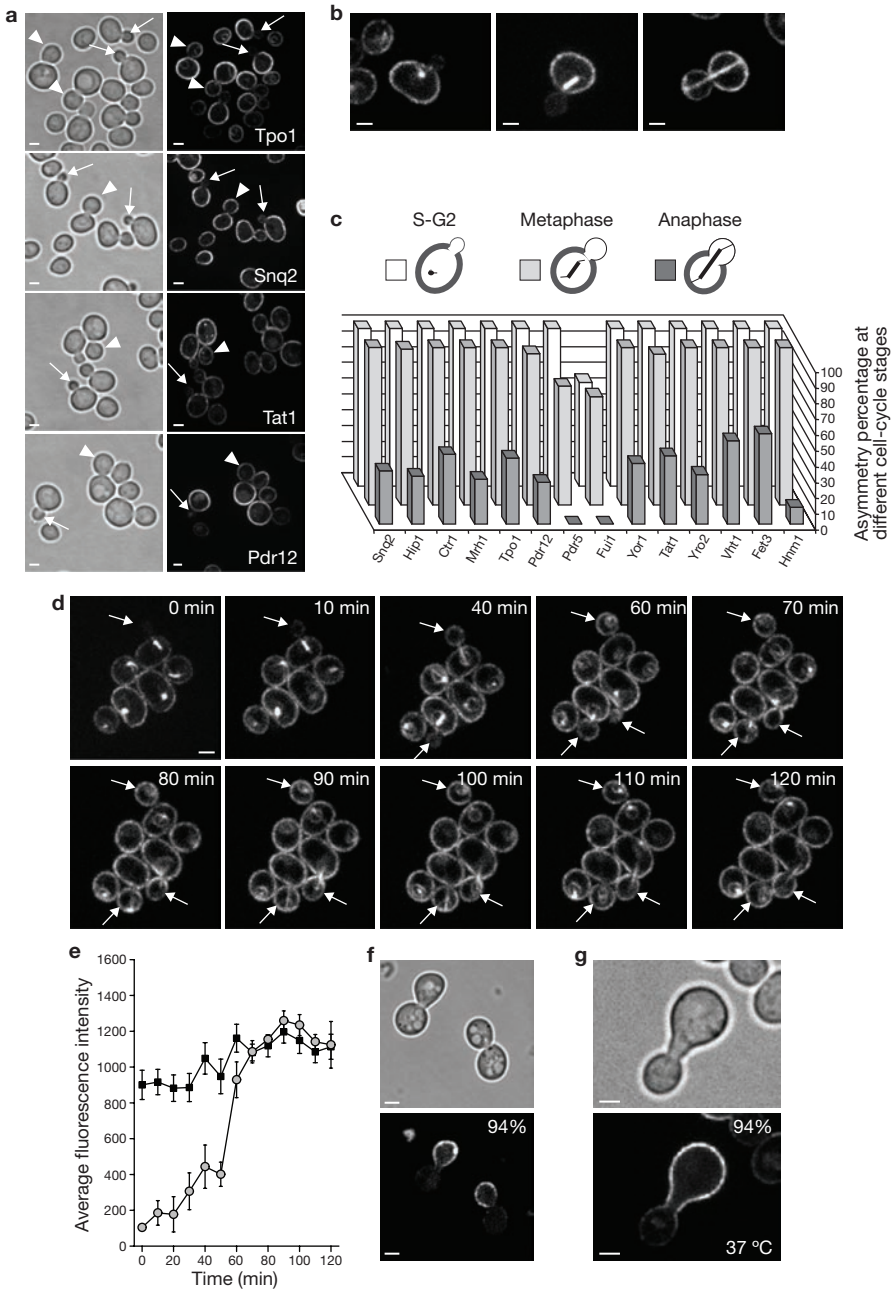

Figure 1 A group of MDR transporter proteins are asymmetrically localized to the mother cortex in a cell-cycle-regulated manner. (**a**) Representative images showing the asymmetric localization of different GFP-tagged MDR transporters to the mother cortex in small budded cells and loss of this asymmetry in larger budded cells. White arrows point to small buds with no GFP-tagged transporters and arrowheads point to larger budded cells with GFP-tagged transporters in the bud. Images displayed on the left are visualized with phase contrast microscopy, images on the right are the same cells visualized with fluorescence microscopy. (**b**) Representative fluorescence microscopy images of cells expressing Tpo1–GFP and GFP–Tub1 (as a marker for the spindle length and hence cell cycle stage), which show that Tpo1–GFP is localized asymmetrically in cells during the S–G2 and M phases and that this asymmetry is lost in anaphase cells. (**c**) Quantification of cells displaying asymmetric transporter localization towards the mother cell ($n > 200$ cells) in populations with specific spindle morphologies. (**d**) Tpo1 localization changes during the cell cycle. Montage of fluorescence microscopy images of cells expressing Tpo1–GFP and GFP–Tub1 at indicated times (see also Supplementary Information, Movie S1). White arrows highlight small buds — that when first formed have asymmetric Tpo1 localization — though different cell-cycle stages. (**e**) Fluorescence intensity of Tpo1–GFP on the cortex of the mother cells (squares) and in the bud cells (circles) over time, as recorded from Supplementary Information, Movie S1. Values indicate the means ± s.e.m. from three different cells. (**f**–**g**) Asymmetric Tpo1–GFP distribution in cells arrested in metaphase by using nocodazole (**f**, average cortex fluorescence intensity $I_{bud}/I_{mother} = 0.2$, $n = 17$) or by maintaining cells carrying the temperature-sensitive allele, *cdc23-1*, at 37 °C (**g**, $I_b/I_m = 0.17$, $n = 22$). Top images are visualized by phase contrast microscopy, bottom image are the same cells visualized by fluorescence microscopy. Scale bars, 2 μm.

metaphase[11]. We confirmed this expression timing for *TPO1* by performing quantitative RT–PCR (using *SWI5* as a metaphase marker[12]) and by simultaneously tracking the timing of budding and changes in nuclear morphologies (Fig. 2a–c). Such restricted expression timing may underlie the lack of MDR proteins in the growing bud and the appearance of MDR proteins in the mature bud before cytokinesis. To test this, we

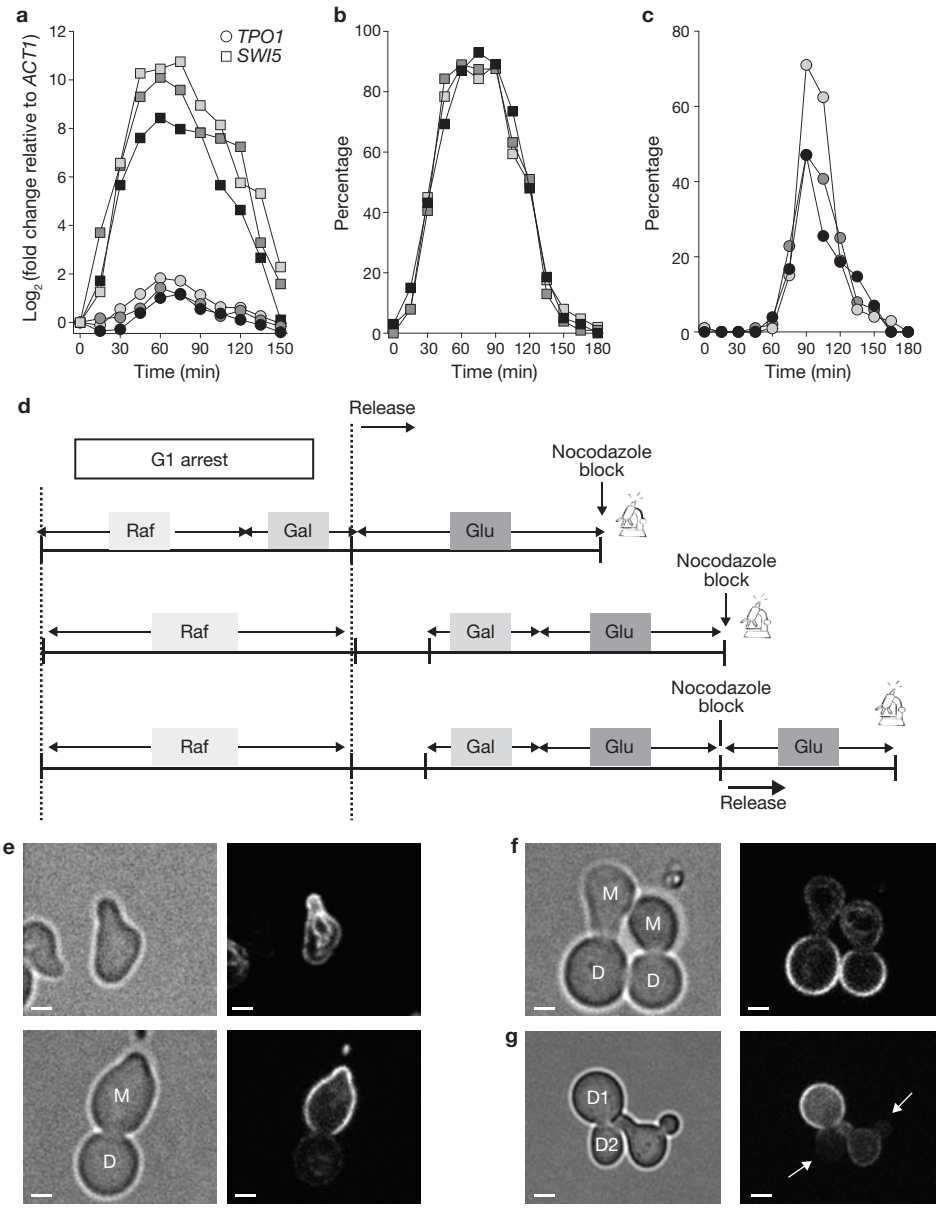

Figure 2 The timing of *TPO1* expression during the cell cycle is critical to the observed localization patterns. (**a**) Total RNA at different time points was purified from cells released from G1 arrest. Using cDNA generated from total RNA, quantitative PCR (qPCR) confirmed that the expression of *TPO1* (circles) peaks at M phase, as shown by comparison with the expression profile of the metaphase-marker gene, *SWI5* (squares). Three biological replicates are shown. (**b**–**c**) Cell-cycle progression was tracked by the budding index (**b**) and nuclear division kinetics (**c**) for the three biological replicates used for RNA purification in the quantitative RT–PCR analyses. (**d**) Schematic showing the experimental design for pulse-expression of Tpo1–GFP with the *GAL1* promoter at different cell-cycle stages in cell cultures synchonized in G1 with the α-mating factor. Top row: pulse expression in G1, middle row: pulse expression in S/M and bottom row: pulse expression in S/M followed by release from the nocodazole block. (**e**) Pulse expression of Tpo1–GFP in G1 (top panels) resulted in asymmetric localization towards the mother after bud formation (in 96% of cells, $n = 26$; bottom panels). M: mother; D: daughter. The mother can be distinguished from the bud (daughter), owing to the shmoo shape caused by pheromone arrest. On the left are phase contrast microscopy images and on the right are the same cells imaged with fluorescence microscopy. (**f**–**g**) Pulse expression of Tpo1–GFP in S/M phases resulted in asymmetric localization towards the bud (in 94% of cells, $n = 34$; **f**), and on further release of the budded cells from the nocodazole block, the bud (D2) of the first daughter cell (D1) was completely devoid of Tpo1–GFP (in 100% of cells, $n = 36$; **g**). Arrows in **g** indicate second bud generation after release from Nocodazole. On the left are phase contrast microscopy images and on the right are the same cells imaged with fluorescence microscopy. Scale bars, 2 μm.

integrated the inducible *GAL1* promoter in front of the Tpo1–GFP gene in the genome so that the sole source of Tpo1–GFP was under the control of this promoter. Using cell populations synchronized in G1 phase by treatment with pheromone, we performed pulse expression (Tpo1–GFP expression was induced with galactose for 30 min, followed by rapid repression with glucose) at G1 or S phase of the cell cycle (Fig. 2d). Nocodazole was present in the release media, and hence the cells eventually arrested in the first metaphase. As predicted, pulse expression in G1 resulted in Tpo1–GFP exclusion from the bud after the release from the G1 arrest (Fig. 2e), whereas pulse expression immediately after the

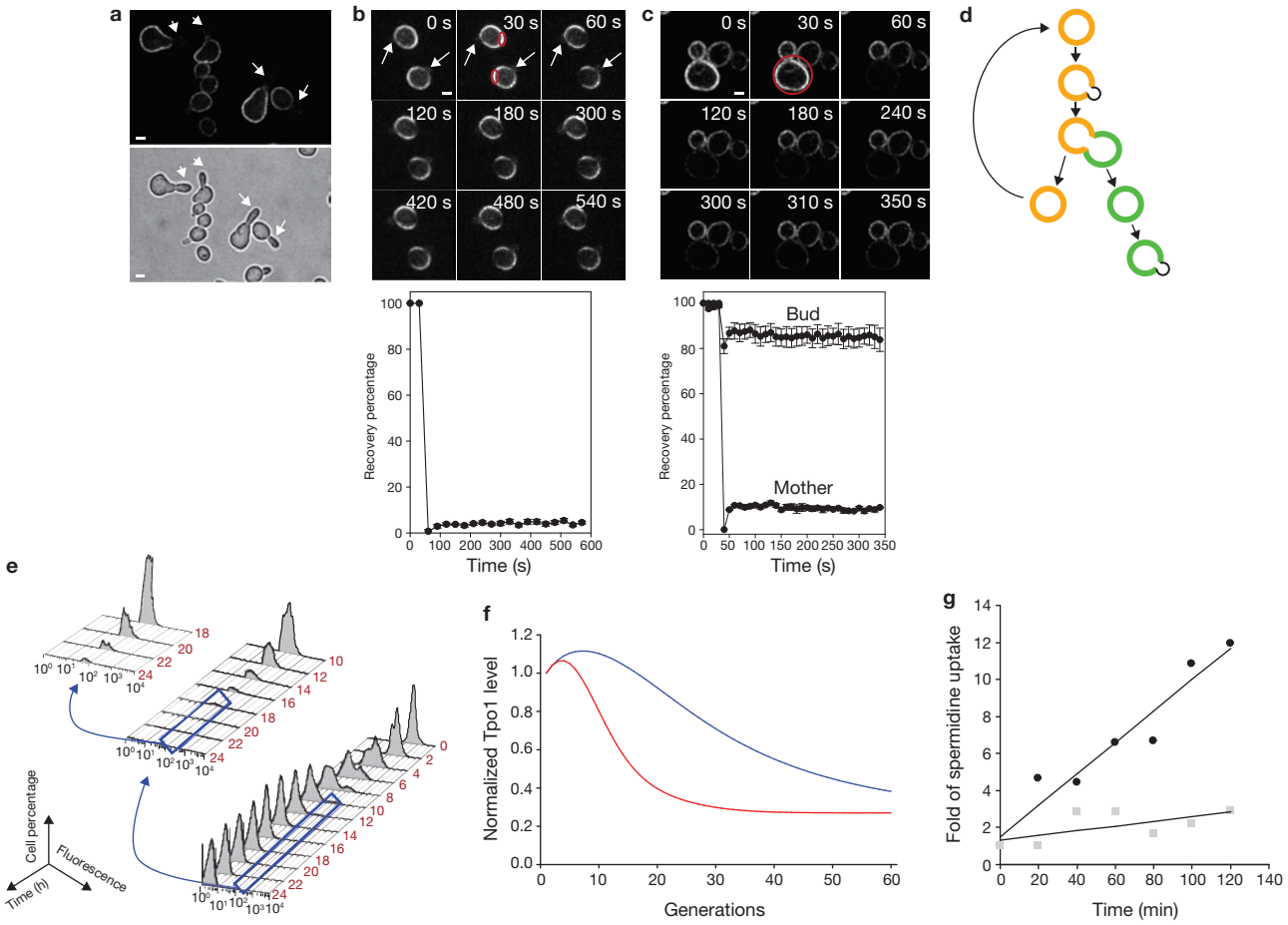

Figure 3 Stable inheritance, protein abundance and activity changes of Tpo1 during RLS. (**a**) Septin mutant *cdc12-6* grown at 37 °C for 1 h to disrupt the septin ring maintained asymmetric localization of Tpo1 to the mother cortex. Note that cells developed the elongated buds (as indicated by the arrows) typical of septin-deficient cells. Top panel is an image visualized with fluorescence microscopy, bottom are the same cells visualized with phase contrast microscopy. Scale bars, 2 μm. (**b**–**c**) FRAP analysis of Tpo1–GFP demonstrating a lack of diffusion in the membrane (**b**) or exchange between the mother and the bud (**c**). In **b**, a small section of the mother cortex (red circle) of two cells with small buds (arrows) was photobleached. A montage of the movie, with images taken at the indicated times, and quantification of fluorescence recovery as a percentage of the pre-bleached level (bottom) are shown. In **c**, the entire cortex of the mother cell was photobleached (red circle) and montage of the movie (top) and quantification (bottom) as in (**b**) are shown. The bud fluorescence was also plotted showing no loss after bleaching of the mother. Error bars represent s.e.m. (**b**, $n = 9$ and **c**, $n = 5$). Scale bars, 2 μm. (**d**) Schematic showing asymmetric inheritance of different pools of MDR protein during each cell division. Orange represents the original pool of MDR proteins in the mother cell. At anaphase, a new pool of MDR proteins (green) is synthesized but is mostly deposited into the bud, the new cell to be. (**e**) Examination of Tpo1–GFP stability by FACS. Cells expressing Tpo1–GFP under the control of the *GAL1* promoter were treated with glucose after 3 h of growth to repress expression, and GFP stability was then assessed by examining the distribution of fluorescence in the population at the indicated time points. Owing to the reduction in cells expressing GFP, the blue boxed areas indicated on a graph have been redrawn as indicated by the arrow with an altered scale on the *y* axis to show the reduced peaks. At the start of the chase the entire population was expressing GFP, but as a result of asymmetric division and retention of Tpo1–GFP in the mother cells, all subsequent newborn cells do not express GFP (low fluorescence). (**f**) Simulation of Tpo1 level change (blue) and activity decay (red) over a cell's RLS. Tpo1 level was modelled based on estimates of the length of the cell cycle from absorbance measurements of cultures, decay rate of the protein because of turnover and loss during cell division estimated from **e**, and amount synthesized based on changes in fluorescence from Supplementary Information, Movie S1. Activity decay was modelled based on similar estimates of cell cycle length and protein turnover, as well as an estimates of the decay rate of activity based on experiments shown in **g**. See Methods for full derivations of the equations used in the simulation. (**g**) Spermidine uptake, at pH 7.2, for equal-dry-weight, young (black circles) and old (grey squares) cell populations sorted by elutriation from the same culture (see Supplementary Information, Fig. S2d for the profile of the old and young generations). Fold uptake was calculated by normalizing the data with respect to the 0 min time point for each population.

release from the G1 arrest resulted in localization of Tpo1–GFP in the bud, probably as a result of polarized secretion (Fig. 2f). These results support the hypothesis that the timing of expression for Tpo1 is crucial for its observed pattern of localization.

Strikingly, when cells with bud-localized Tpo1 (because of pulse expression in S phase) were followed into the subsequent cell cycle after release from the nocodazole arrest, the newly formed buds (D2 in Fig. 2g) were completely devoid of Tpo1, suggesting that the Tpo1 protein expressed in the previous cycle was tightly sequestered by the mother cortex. We first thought that this might be because of the septin diffusion barrier at the bud neck[13]. However, after shifting a septin mutant (*cdc12-6*; ref. 14) to the non-permissive temperature for 1 h, Tpo1 in the mutant cells was still retained in the mother and no protein was observed in the buds (which were abnormally elongated, a characteristic

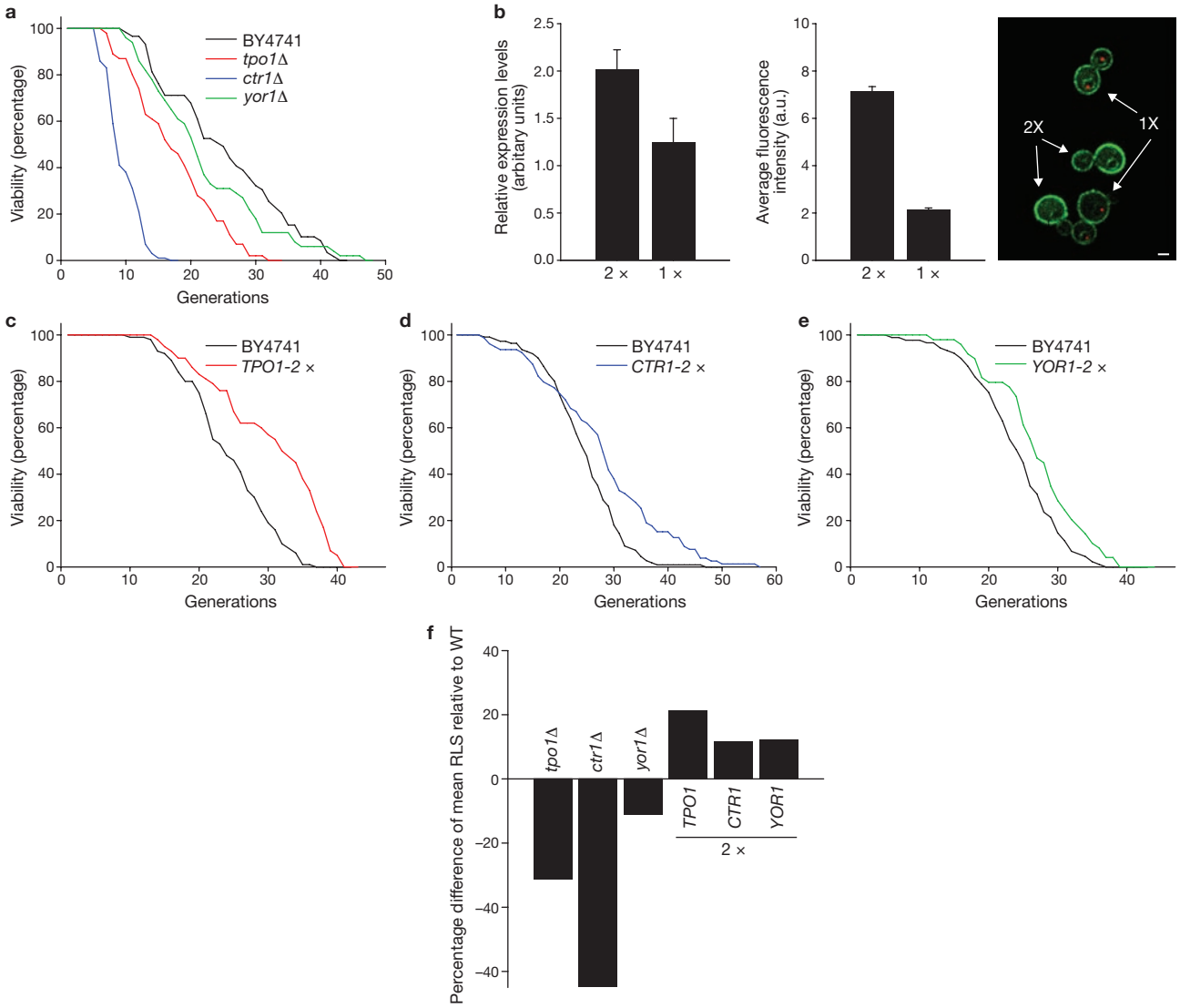

Figure 4 Levels of different MDR transporters affect the replicative lifespan. (**a**) Viability curves of strains with deletions of different MDR transporters (*tpo1Δ*, *ctr1Δ* or *yor1Δ*, in **a**-mating-type strains) from a single representative experiment. Deletion of any of the MDR transporters reduced RLS relative to the wild-type **a**-mating-type strain (BY4741; for α-mating-type strain analysis, see Supplementary Information, Fig. S3b–d and Table S2). (**b**) An extra copy of *TPO1* increases *TPO1* expression, as shown by qPCR (left) and Tpo1–GFP cortical fluorescence intensity (right). Representative images are shown of Tpo1–GFP in cells with 1 × Tpo1–GFP (specifically marked with the spindle pole body marker Spc42–mCherry) or 2 × Tpo1–GFP observed in the same field. Error bars represent s.e.m. ($n > 100$). Scale bar, 2 μm. (**c**–**e**) Viability curves from representative experiments, which show that introduction of an extra copy of *TPO1*, *CTR1* or *YOR1* extends RLS relative to wild type (BY4741). (**f**) The effect of deletion or addition of one extra copy of *TPO1*, *CTR1* or *YOR1* on RLS, as represented by the percentage difference of mean RLS relative to that of the corresponding wild-type control strain (**a**-mating type). Table S2 (Supplementary Information) shows additional results for both mating-type strains.

of septin loss; Fig. 3a). To test if Tpo1 was simply unable to diffuse in the membrane, fluorescence recovery after photobleaching (FRAP) was performed, whereby a section of the mother cortex was photobleached. No recovery was observed for the duration of the imaging (10 min), suggesting that Tpo1 was tightly bound to the mother cell cortex (Fig. 3b, Supplementary Information, Movie S2). Similarly, photobleaching of the entire mother cell in a large-budded cell did not show fluorescence recovery in the mother, whereas the bud maintained its fluorescence, suggesting a lack of exchange of Tpo1 between the mother and the bud (Fig. 3c, Supplementary Information, Movie S3). FRAP experiments also confirmed the same stable inheritance for two other MDR proteins, Ctr1 and Yor1 (Supplementary Information, Fig. S1b).

These results suggest that whereas the mother cell keeps its own pool of MDR proteins, the daughter cell inherits the majority of the newly synthesized MDR proteins during mitosis, and the new and aged proteins are stably segregated along the bud–mother axis (Fig. 3d). This implies that a cell receives most of the MDR proteins at its birth, and as the cell undergoes subsequent divisions, its pool of MDR proteins is only slightly replenished during each anaphase, because the majority of the new protein is deposited into the bud. Meanwhile, the ageing MDR protein population is retained in the mother and restricted from entering the bud. Depending on the rate of decay of these proteins, their level and/or activity could eventually decline as the mother cell advances in replicative age. As such, MDR transporters may fit the criteria as

beneficial components of the cell, which as they then deteriorate are recessive determinants of a cell's RLS.

To quantitatively assess this hypothesis, we modelled the dynamics of the MDR protein population over a yeast cell's RLS. The model assumes deposition of newly synthesized MDR protein at a cell's birth. This protein pool follows a decay rate of α and is poorly replenished with newly synthesized protein (amount β, assessed as a fraction of the first pool) during each subsequent anaphase (See Methods). To estimate α, Tpo1 expression was induced from the *GAL1* promoter for 3 h and then repressed by addition of glucose, and the stability of Tpo1–GFP was monitored using fluorescence-activated cell sorting (FACS). As shown in Fig. 3e (and Supplementary Information, Fig. S2a), as the culture underwent exponential growth, the fraction of cells expressing GFP decreased rapidly, but did remain observable for the duration of the experiments (24 h, approximately 14 divisions), consistent with stable inheritance of the pulse-expressed fluorescent protein in the original population. An exponential fitting of mean fluorescence within the fluorescent cell population led to an estimate of the decay rate α to be 0.16 h^{-1} (Supplementary Information, Fig. S2b, c). β was estimated to be on average 0.27 by quantification of mother cell fluorescence increase as a fraction of fluorescence deposition in the daughter from a time-lapse microscopy movie (Supplementary Information, Movie S1).

Model simulation showed a non-monotonic change of Tpo1 level as a function of the cell's replicative age: the level increased initially and then gradually declined for the duration of the RLS (Fig. 3f, blue line). A factor contributing to the time-dependent change in Tpo1 level during RLS is a slow but gradual increase in cell cycle length as observed in many studies[15,16], which results in slowed replenishment, while the decay rate remains constant. In addition to a diminishing protein level, transporter molecules present in older cells are expected to be, on average, older than those in younger cells, which may result in reduced functionality. As Tpo1 is a major polyamine transporter in the cell, to examine if polyamine transport activity was indeed altered in older cells when compared with younger cells, we used an elutriation protocol[17] to isolate populations enriched for young or old cells (Supplementary Information, Fig. S2d). The polyamine transport activity was assayed by using radioactive spermidine[18]. As shown in Figure 3g, the older cell population exhibited a considerable reduction in polyamine transport activity. Activity decay can be modelled with an additional rate, estimated from the result in Figure 3g (see Methods). Accounting for the functional decay predicts an even sharper decline of the overall polyamine transporter activity over the RLS (Fig. 3f, red line), which approaches a minima around 20–30 generations.

Substrates of MDR transporters have been implicated in ageing. For example, polyamines are known to have an important role in the lifespan of a variety of cell types, including yeast[19,20]. Ctr1 is a major transporter of the copper ion, an essential cofactor for superoxide dismutase, an enzyme critical for protecting cells against oxidative damage and for normal lifespan[21]. Yor1 confers resistance to many organic acids[22], including acetic acid, a product of fermentative metabolism and a key factor in chronological ageing[23]. To determine if MDR proteins have any function in RLS, we used a micromanipulation assay[24] to measure the RLS of mutant cells bearing gene deletion for *TPO1*, *YOR1* or *CTR1*. None of the mutations seemed to cause any drastic growth defect in actively dividing populations, expected to be composed mostly of young cells (Supplementary Information, Fig. S3a), although these mutations could have subtle effects on cellular physiology. **a**-Mating-type cells carrying *ctr1Δ* exhibited a markedly reduced RLS (by 66.4%, $P < 0.001$) when compared with wild-type cells, whereas *tpo1Δ* reduced RLS by 31.5% ($P < 0.001$) and *yor1Δ* reduced RLS by 11.3% ($P < 0.06$) (Fig. 4a). Qualitatively similar observations were made for α-mating-type cells carrying *ctr1Δ* (95% reduction, $P < 0.001$) and *yor1Δ* (15.8% reduction, $P < 0.002$). The lifespan of α-mating-type *tpo1Δ* cells was also short when compared with wild-type RLS (8.2% reduction), although the difference was not statistically significant ($P < 0.2$) (Supplementary Information, Fig. S3b–d and Table S2 for detailed RLS data).

An alternative way to test if MDR transporters are limiting factors in RLS determination is to examine if an increased MDR protein level leads to extended RLS. As gross and unregulated over-expression of MDR proteins may have deleterious or pleiotropic effects, we opted to perform this analysis by introducing one extra copy of the *TPO1*, *YOR1* or *CTR1* gene, controlled under the respective native promoter, to the respective genomic locus. A moderate increase in mRNA and protein expression levels in the 2 × *TPO1* strain, compared with those in the wild type, was confirmed by quantitative RT–PCR and fluorescence measurement, respectively (Fig. 4b). Remarkably, introduction of an extra copy of *TPO1*, *YOR1* or *CTR1* to the respective native locus resulted in significant increase in RLS to varying extents, compared with that of the wild type (Fig. 4c–f, Supplementary Information, Fig. S3 and Table S2).

Taken together, the cellular experiments demonstrate that the MDR proteins exhibit a unique asymmetric inheritance pattern as a result of their timed expression in the cell cycle, localized deposition, and stable association with the cortex, which suggests that these proteins are markers of cellular replicative ageing in asymmetrically dividing yeast cells. Analysis using a polyamine transporter (Tpo1) suggested a slow protein turnover and a decline in the transporter activity during RLS. Measurements of RLS provide further functional evidence that these transporter proteins are ageing determinants: even individual deletion of the MDR genes could lead to shortened RLS, whereas a moderate increase in the expression of one of the three tested transporters (because of an extra copy of the gene) led to extended RLS. Thus, in addition to deleterious, dominant ageing factors, MDR proteins represent a class of recessive, beneficial factors that limit RLS. Interestingly, the dominant and recessive factors may represent two sides of the same process: as ageing cells accumulate materials that may interfere with normal cellular processes, such as ERC and oxidatively damaged proteins[1], diminution of the protective functions provided by MDR proteins may exacerbate the progress towards cell death induced by toxic agents. In turn, environmental or physiological factors, such as calorie restriction or stress, could impact the ageing process[25,26] by lessening the production of the toxic substrates of MDR transporters, such as organic acids, or the need for importing protective substrates, such as polyamines[27].

Many interesting questions remain for future study, including what the relevant substrates are of the MDR transporters that affect ageing, and how changes in the level of MDR proteins interact with other well studied pathways of cellular replicative ageing. Finally, several mammalian ABC transporters are well known stem-cell markers and are down-regulated at the time of differentiation[28]. It has been hypothesized that these transporter proteins are particularly important for maintaining the long-term proliferative potential of stem cells. It will be interesting to investigate if MDR transporter proteins are also segregated asymmetrically during stem cell divisions and have any role in ageing and senescence in multicellular organisms.

METHODS

Methods and any associated references are available in the online version of the paper at http://www.nature.com/naturecellbiology/

Note: Supplementary Information is available on the Nature Cell Biology website

ACKNOWLEDGMENTS

We thank C. Zhou for assistance on RLS experiments; C. Seidel and B. Fleharty for help on RNA purification and quantitative RT–PCR; R. Zhu, K. Wagner and J. Haug for assistamce with cell-sorting experiments and B. Slaughter, N. Pavelka and S. Xia for technical advice and critical comments. This research is supported by the National Institutes of Health, grant R01GM057063 to R.L. The content is solely the responsibility of the authors and does not necessarily represent the official views of the National Institute of General Medical Sciences or the National Institutes of Health.

AUTHOR CONTRIBUTIONS

A.E. performed all of the experiments and prepared the manuscript figures and draft. G.R. contributed to MDR protein quantification and RLS measurements. B.R. constructed the mathematical model for MDR dynamics during RLS. P.P. and V.C. provided technical assistance for various experiments. R.L. conceived and supervised the project and revised the manuscript.

COMPETING FINANCIAL INTERESTS

The authors declare no competing financial interests.

Published online at http://www.nature.com/naturecellbiology
Reprints and permissions information is available online at http://npg.nature.com/reprintsandpermissions/

1. Henderson, K. A. & Gottschling, D. E. A mother's sacrifice: what is she keeping for herself? *Current Opinion in Cell Biology* **20,** 723–728 (2008).
2. Steinkraus, K. A., Kaeberlein, M. & Kennedy, B. Replicative aging in yeast: the means to the end. *Annu. Rev. Cell Dev. Biol.* **24,** 29–54 (2008).
3. Mortimer, R. K. & Johnston, J. R. Lifespan of individual yeast cells. *Nature* **183,** 1751–1752 (1959).
4. Erjavec, N., Larsson, L., Grantham, J. & Nystrom, T. Accelerated aging and failure to segregate damaged proteins in Sir2 mutants can be suppressed by overproducing the protein aggregation-remodeling factor Hsp104p. *Genes Dev.* **21,** 2410–2421 (2007).
5. Sinclair, D.A. & Guarente, L. Extrachromosomal rDNA circles — a cause of aging in yeast. *Cell* **91,** 1033–1042 (1997).
6. Park, H.-O. & Bi, E. Central roles of small GTPases in the development of cell polarity in yeast and beyond. *Microbiol. Mol. Biol. Rev.* **71,** 48–96 (2007).
7. Huh, W.-K. *et al.* Global analysis of protein localization in budding yeast. *Nature* **425,** 686–691 (2003).
8. Ernst, R., Klemm, R., Schmitt, L. & Kuchler, K. Yeast ATP-binding cassette transporters: cellular cleaning pumps. *Methods Enzymol.* **400,** 460–484 (2005).
9. Uemura, T., Tachihara, K., Tomitori, H., Kashiwagi, K. & Igarashi, K. Characteristics of the polyamine transporter TPO1 and regulation of its activity and cellular localization by phosphorylation. *J. Biol. Chem.* **280,** 9646–9652 (2005).
10. Burke, D. J. & Church, D. Protein synthesis requirements for nuclear division, cytokinesis, and cell separation in *Saccharomyces cerevisiae*. *Mol. Cell. Biol.* **11,** 3691–3698 (1991).
11. Spellman, P. T. *et al.* Comprehensive identification of cell cycle-regulated genes of the yeast *Saccharomyces cerevisiae* by microarray hybridization. *Mol. Biol. Cell* **9,** 3273–3297 (1998).
12. Althoefer, H., Schleiffer, A., Wassmann, K., Nordheim, A. & Ammerer, G. Mcm1 is required to coordinate G2-specific transcription in *Saccharomyces cerevisiae*. *Mol. Cell. Biol.* **15,** 5917–5928 (1995).
13. Faty, M., Fink, M. & Barral, Y. Septins: a ring to part mother and daughter. *Curr. Genet.* **41,** 123–131 (2002).
14. Barral, Y., Mermall, V., Mooseker, M. S. & Snyder, M. Compartmentalization of the cell cortex by septins is required for maintenance of cell polarity in yeast. *Mol. Cell* **5,** 841–851 (2000).
15. Egilmez, N. K. & Jazwinski, S. M. Evidence for the involvement of a cytoplasmic factor in the aging of the yeast *Saccharomyces cerevisiae*. *J. Bacteriol.* **171,** 37–42 (1989).
16. Egilmez N. K., Chen, J. B. & Jazwinski S. M. Preparation and partial characterization of old yeast cells. *J. Bacteriol.* **45,** b9–b17 (1990).
17. Lesur, I. & Campbell, J. L. The transcriptome of prematurely aging yeast cells is similar to that of telomerase-deficient cells. *Mol. Biol. Cell* **15,** 1297–1312 (2004).
18. Tomitori, H. *et al.* Multiple polyamine transport systems on the vacuolar membrane in yeast. *Biochem. J.* **353,** 681–688 (2001).
19. Eisenberg, T. *et al.* Induction of autophagy by spermidine promotes longevity. *Nat. Cell Biol.* **11,** 1305–1314 (2009).
20. Morselli E. *et al.* Autophagy mediates pharmacological lifespan extension by spermidine and resveratrol. *Aging* **1,** 961–970 (2009).
21. Kirchman, P. A. & Botta, G. Copper supplementation increases yeast life span under conditions requiring respiratory metabolism. *Mech. Ageing Dev.* **128,** 187–195 (2007).
22. Cui, Z., Hirata, D., Tsuchiya, E., Osada, H. & Miyakawa, T. The multidrug resistance-associated protein (MRP) subfamily (Yrs1/Yor1) of *Saccharomyces cerevisiae* is important for the tolerance to a broad range of organic anions. *J. Biol. Chem.* **271,** 14712–14716 (1996).
23. Burtner, C., Murakami, C., Kennedy, B. & Kaeberlein, M. A molecular mechanism of chronological aging in yeast. *Cell Cycle* **8,** 1256–1270 (2009).
24. Steffen, K.K., Kennedy, B. K. & Kaeberlein, M. Measuring replicative life span in the budding yeast. *J. Vis. Exp.* **28,** doi: 10.3791/1209 (2009).
25. Chen, D. & Guarente, L. SIR2: a potential target for calorie restriction mimetics. *Trends Mol. Med.* **13,** 64–71 (2007).
26. Merry, B.J. Oxidative stress and mitochondrial function with aging—the effects of calorie restriction. *Aging Cell* **3,** 7–12 (2004).
27. Igarashi, K. & Kashiwagi, K. Polyamines: mysterious modulators of cellular functions. *Biochem. Biophys. Res. Commun.* **271,** 559–564 (2000).
28. Bunting, K. D. ABC Transporters as phenotypic markers and functional regulators of stem cells. *Stem Cells* **20,** 11–20 (2002).

DOI: 10.1038/ncb2085

METHODS

Yeast strains and genetic methods. Yeast cell culture and genetic manipulations were performed as previously described[29]. All yeast strains were derivatives of the S288c background and are listed in Supplementary Information, Table S3. To generate strains expressing an extra copy of *TPO1*, *YOR1* or *CTR1*, the wild-type strain BY4741 was transformed with an integrative plasmid (pRS305) carrying an extra copy of the gene of interest, along with its own promoter. Transformants were screened on plates lacking Leu and proper integration was checked by PCR for each strain. For imaging analysis of the 2 × Tpo1–GFP strain, an extra copy of the Tpo1–GFP cloned into the same integrative plasmid was transformed to RLY3785 strain (1 × Tpo1–GFP).

Fluorescence microscopy and image quantification. Confocal microscopy imaging was carried out on an inverted Zeiss 200M microscope with a ×100 oil immersion objective fitted with a spinning disc confocal microscopy system (Yokagawa) and an electron multiplying charged coupling device (EM-CCD; Hamamatsu C9100) at 25 °C. FRAP data were acquired with this system using an attached Micro-point Mosaic bleaching system (Photonic Instruments), integrated with Metamorph acquisition software (Molecular Devices). Overnight cultures expressing Tpo1–GFP in synthetic medium were harvested and A_{600} was adjusted to 0.3. Cultures were incubated at 30 °C for 2 h. Agarose pad (20%; w/v) composed of the same medium was used for longer analysis. In FRAP experiments, part or the whole mother cell cortex was bleached with a 1.8 ms pulse of laser at 488 nm. Fluorescence recovery was monitored over the indicated time range. Fluorescence intensity was analysed using ImageJ software (National Institutes of Health) and fluorescence recovery as a percentage of fluorescence intensity before photobleaching was plotted against time.

RT–PCR analysis. For quantitative RT–PCR, total RNA was purified, using samples from different time points after release from G1-arrest (Fig. 2a), using the hot-acid-phenol method, followed by isopropanol precipitation. After DNase (Applied Biosystems) treatment, RNA was converted to cDNA using reverse transcriptase (Invitrogen). A Corbett robot (Corbett Life Science) was used to load PCR reactions in 384-well plate format for analysis on an ABI-7900 (Applied Biosystems). The delta-delta Ct (cycle threshold) method was applied to measure fold differences between *TPO1* or *SWI5* expression relative to *ACT1*, which was used as the loading control[30]. Using TaqMan technology, multiplexed assays designed with Primer Express 3.0 software (Applied Biosystems), were performed with different probes (Integrated DNA Technologies). Three biological replicates were used for analysis.

Tpo1 pulse expression at different cell-cycle stages. A strain (RLY4234, see Supplementary Information, Table S3) was constructed with Tpo1–GFP under the regulation of the *GAL1*-promoter. An overnight culture in raffinose was adjusted to A_{600} 0.3 and cells were arrested at the G1-phase in yeast extract peptone (YEP) medium containing 2% (w/v) raffinose and α-factor (5 μg ml^{-1}) for 2 h. For G1-phase pulse expression of Tpo1–GFP, 2% (w/v) galactose was added to the medium for 30 min during the G1 arrest. Cells were washed twice and released into YEP medium containing 2% (w/v) glucose with 15 μg ml^{-1} nocodazole for 2 h. For S/M-phase pulse expression of Tpo1–GFP, cells were released from G1 arrest into YEP medium containing 2% (w/v) raffinose, until cells started budding. An expression pulse was given in YEP medium containing 2% (w/v) raffinose / galactose with 15 μg ml^{-1} nocodazole for 30 min, followed by transferring into YEP medium containing 2% (w/v) glucose with 15 μg ml^{-1} nocodazole. For the second round of budding, 5 μg ml^{-1} nocodazole was used for arrest and cells were released into YEP medium containing 2% (w/v) raffinose, to allow cells to bud again.

FACS analysis of Tpo1–GFP stability. Yeast strain RLY4234 was grown overnight at 30 °C in raffinose. A_{600} was adjusted to 0.3 in YEP medium containing 2% (w/v) raffinose and galactose and incubated for 3 h (FACS analysis showed 100% of cells were expressing GFP). A_{600} was adjusted to 0.1 in YEP medium containing 2% (w/v) glucose and incubated at 30 °C with 200 rpm shaking. Samples were taken every 2 h for 24 h; dilutions were made to A_{600} 0.1 once A_{600} exceeded 1 to keep cells in the exponential phase. Samples were fixed with 1% (w/v) formaldehyde for 20 min. Using an Influx cell sorter (BD Biosciences) 2×10^6 cells were sorted to determine the percentage of cells expressing GFP in the population. The machine was used to maximum sensitivity (0.03%), which enabled us to trail Tpo1–GFP though 14 generations. Four biological replicates were performed for each analysis.

Determination of yeast RLS. All lifespan analyses were carried out by using micromanipulation as previously described[24] on standard yeast extract-peptone-dextrose (YEPD) plates (2% (w/v) glucose and 2% (w/v) agar), grown at 30 °C. For statistical significance, RLS datasets were analysed by Wilcoxon rank-sum test. For all strains tested, mean RLS and *P* values were calculated from pooled experiments where each strain of interest was compared with its respective wild-type strain, which was examined in the same experiment (for datasets see Supplementary Information, Table S2).

Elutriation and spermidine import assay. Young and old cell populations were sorted using elutriation as previously described[17] and polyamine transport assays for both young and old populations was performed as previously described[18].

Equations for modelling of Tpo1 level and activity change over the cell's RLS. We assume that after i cell cycles a certain amount, β_i, of protein is synthesized. The protein decays with the rate α. The period, τ_i, of the cell cycle is not constant and it grows with the number of cycles[15,16]. Therefore, the time, T_i, measured from the end of the first cell cycle to the end of cycle i is

$$T_i = \sum_{k=2}^{i} \tau_k \qquad (1)$$

and by convention, $T_1 = 0$. The total amount, P_i, of the protein at the end of cycle i is found as a sum of partial protein amounts, $P_k^{(i)}$, each one of which is computed as follows:

$$P_k^{(i)} = \beta_k \exp(-\alpha(T_i - T_k)),\ 1 \le k \le i \qquad (2)$$

and represents the amount of protein, β_k, generated at cycle k, after its degradation has been included, during a timespan of

$$T_i - T_k = \sum_{m=2}^{i} \tau_m - \sum_{m=2}^{k} \tau_m = \sum_{m=k+1}^{i} \tau_m$$

Using equation 2, we obtain

$$P_i = \sum \beta_k \exp(-\alpha(T_i - T_k)) \qquad (3)$$

The initial condition is $P_1 = \beta_1 = 1$ and for simplicity we choose $\beta_i = \beta < 1$ for $i > 1$.

The protein activity, A_i, diminishes with time, so we describe it using activity decrease rate α_1 proportional to the generation number $\alpha_1(k) = a(k-1)$. Thus we have for the protein activity:

$$A_i = \sum_{k=1}^{i} \beta_k \exp\{-\lambda[\alpha + a(k-1)](T_i - T \qquad (4)$$

Parameters Estimate. For estimate of the decay rate α from the FACS data we assume that the mean fluorescence decay is governed by two independent processes, dilution of the Tpo1–GFP population because of cell division and pure protein decay with the rate α. The cell cycle period is denoted as τ. Then the decrease rate, γ, of Tpo1–GFP is found as

$$\gamma = \alpha + \frac{\ln 2}{\tau}$$

and

$$\alpha = \gamma - \frac{\ln 2}{\tau}$$

The cell cycle period, $\tau = 1.6$ h is estimated from absorbance measurements. The fitting of the Tpo1–GFP dynamics data gives $\gamma = 0.59$ h^{-1} and we find $\alpha = 0.16$ h^{-1} (see Supplementary Information, Figure S2b, c).

We model the cell cycle period, τ_i, with a quadratic function

$\tau_i = B_0 + B_1 i + B_2 i^2$.

The parameter values for simulation were chosen to be $B_0 = 1.6$, $B_1 = 0$ and $B_2 = 0.0016$, which corresponds to 1.6 h at the first cell cycle and to 3 h at cell cycle 30.

β was estimated by quantification of Movie S1 (Supplementary Information), as the ratio of increase of fluorescence in mother relative to flourescence deposition in the bud. Taking decay into account, the value of β was found to be on average 0.27.

Figure 3g shows that the protein activity in the young cells (average age of 1 generation) is $r = 6.7$ times higher than that of the older cells (average age of 8 generations). As $(\tau_8 - \tau_1)/\tau_1 \approx 0.06$ we assume for simplicity the constant cell cycle period $\tau = \tau_1$, find the above activity ratio $r = 1/\exp(-56a\tau)$ and obtain $a = \ln 6.7/(56\tau) = 0.021$.

29. Burke, D., Dawson, D., Stearns, T. & Cold Spring Harbor Laboratory. *Methods in yeast genetics: a Cold Spring Harbor laboratory course manual*. (Cold Spring Harbor Laboratory Press, 2000).

30. Livak, K. J. & Schmittgen, T. D. Analysis of relative gene expression data using real-time quantitative PCR and the 2-[Delta][Delta]CT Method. *Methods* **25,** 402–408 (2001).

nature cell biology

DOI: 10.1038/ncb2085

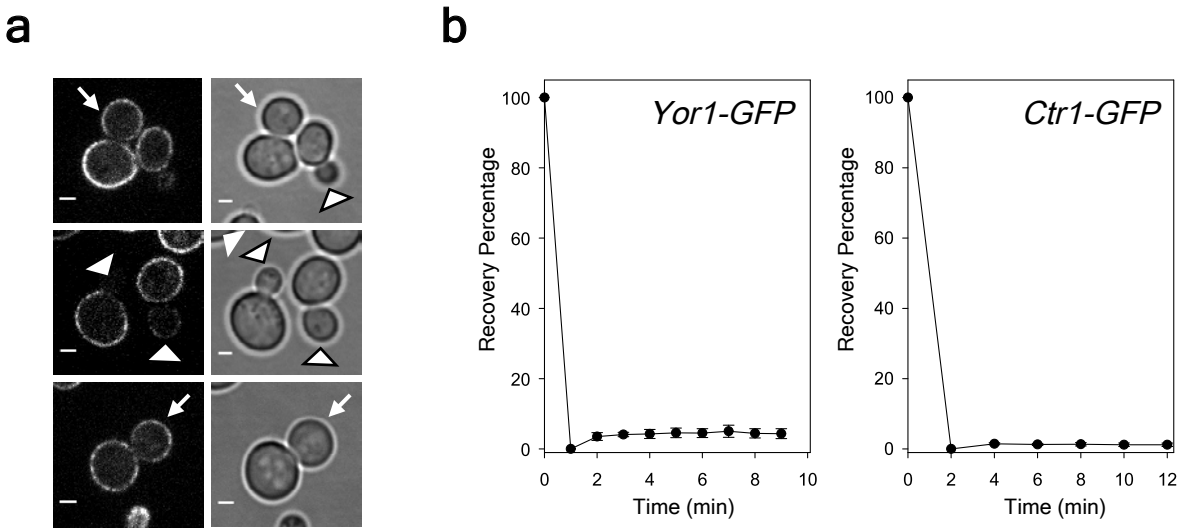

Figure S1 Additional data characterizing Tpo1 localization and dynamics. **a,** N-terminus GFP-Tpo1, expressed from the Tpo1 genomic locus under the native promoter, asymmetrically localize to the mother cortex during polarized growth. Arrowheads point to small buds with no GFP-Tpo1; White arrows point to large-budded cells with GFP-Tpo1 in the bud. **b,** FRAP analysis of Yor1-GFP and Ctr1-GFP showing stable retention of both proteins on the cell cortex. A small section of the cell cortex was photobleached and quantification of fluorescence recovery as a percentage of the pre-bleached level is shown. Error bars represent SEM.

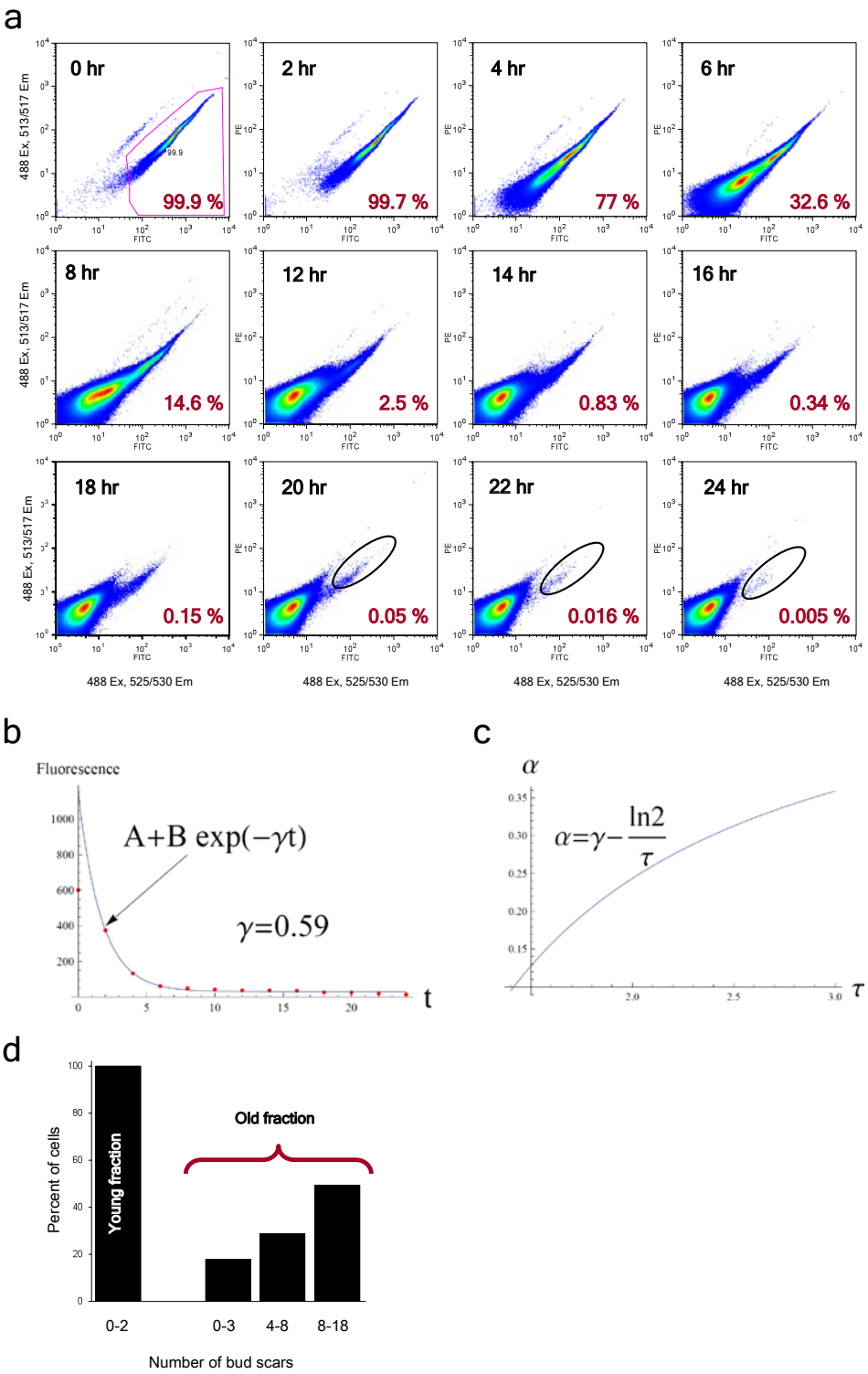

Figure S2 Tpo1 stability and decay throughout the replicative life span. **a,** FACS analysis to determine the percentage of GFP⁺ cells after *TPO1*-GFP pulse expression from the *GAL1* promoter (Experiment details in Fig. 3f). Samples were taken for sorting ($2X10^6$ cells) every 2 hrs for a total of 24 hrs. Percentage of GFP⁺ cell was determined using the same gates established at the initial sample (zero hr, 100% GFP⁺) throughout the whole analysis. **b,** Exponential fitting of Tpo1-GFP dynamics revealed that the fluorescence decrease rate γ=0.59; **c**, The mathematical relationship between protein decay rate α and the cell cycle period τ in the FACS analysis. **d,** Calcofluor staining showing the generation profile (as represented by the number of bud scars) of two cell fractions, young and old, sorted by elutriation.

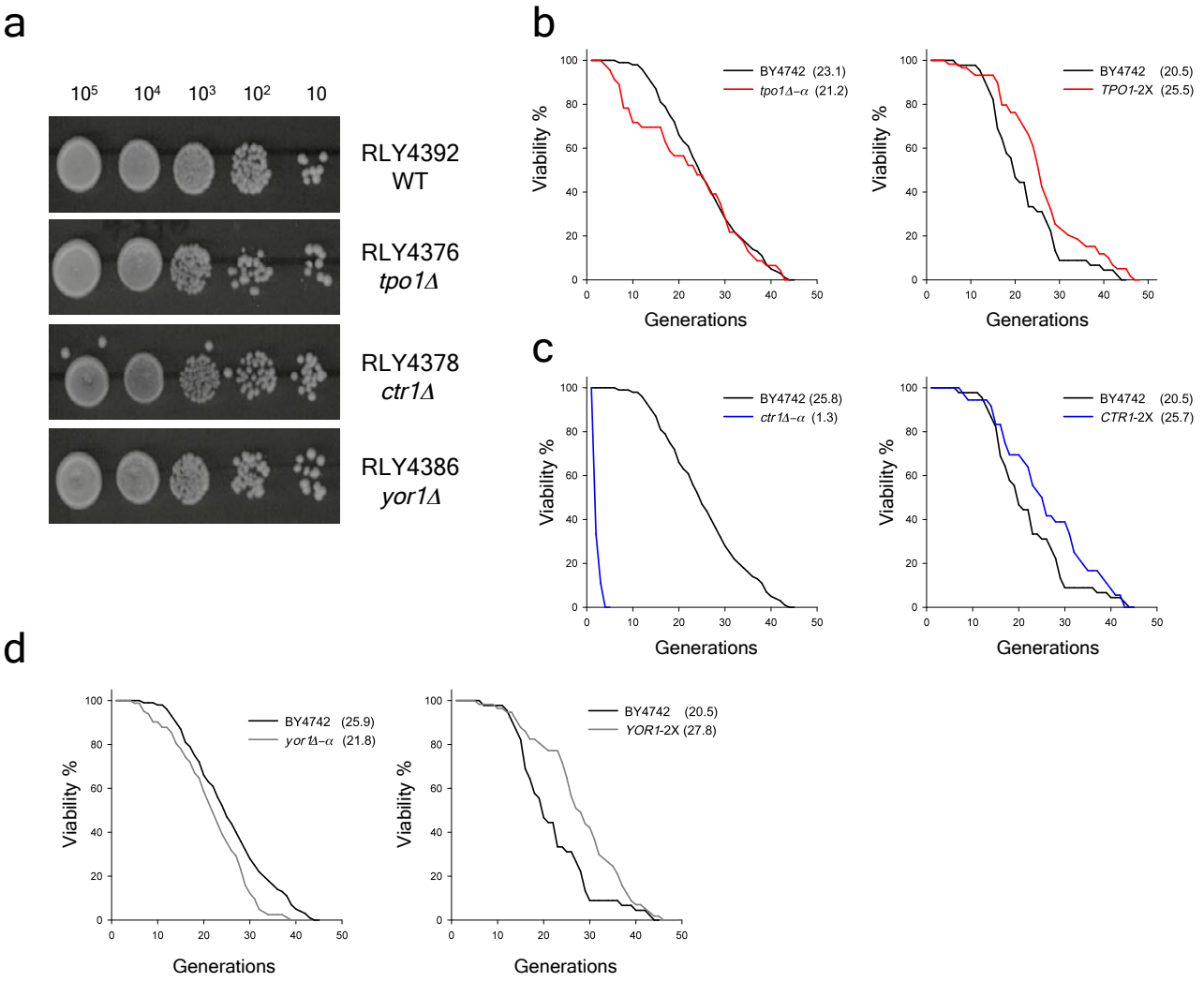

Figure S3 Deletion of MDR transporters affect RLS without causing a growth defect. **a,** Growth assay of wild-type and deletions of the transporters Tpo1, Yor1 and Ctr1. Cultures of different strains exponentially growing in YPD at 30 ºC were serially diluted and spotted (4 µl) on YPD plates at 30 ºC for 2 days. **b-d,** RLS viability curves for different deletions and extra copy strains of Tpo1, Yor1 and Ctr1. Mean RLS for each strain is shown between parentheses, for complete summary see Supplementary Table 2.

Supplementary Movie legends

Movie S1 Tpo1p asymmetric localization to the mother cortex.

Movie S2 FRAP analysis of Tpo1-GFP on the mother cortex showing no fluorescence recovery for the duration of the movie imaging. Also see Figure 3b in the main text.

Movie S3 Photobleaching Tpo1-GFP on the whole mother cortex, showing no fluorescence recovery during the movie. Also see Figure 3c in the main text.

Table S1. MDR transporters asymmetrically localizing to the mother cell during polarized growth

Protein	Function
Ctr1	High affinity copper transporter
Fet3	Oxidoreductase required for high affinity iron uptake
Fui1	High affinity uridine permease
Hip1	High affinity histidine permease
Hnm1	Choline/Ethanolamine transporter
Mrh1	Membrane protein similar to Hsp30 and Yro2
Pdr5	Multidrug ABC-transporter
Pdr12	Multidrug ABC-transporter
Snq2	Multidrug ABC-transporter
Tat1	Amino acid transporter
Tpo1	Polyamine transporter
Vht1	High affinity vitamin H symporter
Yor1	Multidrug ABC-transporter
Yro2	Stress-related transporter of unknown function

Table S2. Summary of replicative life span analysis. Mean replicative life span for each strain was determined and matched to the wild type cells examined on the same experiment. For statistical significance, P-values were determined using Wilcoxon rank-sum test. Each "wild-type" was examined along side the mutant strain in the row below.

Genotype	Mating type	Mean RLS	%	# of cells	P-value
Wild-type	a	23.8		62.0	
	α	23.1		91	
tpo1Δ	a	16.3	-31.5	41	6.2E-04
	α	21.2	-8.2	47	1.3E-01
Wild-type	a	23.8		62	
	α	25.8		44	
ctr1Δ	a	8.0	-66.4	20 (89)	1.0E-08
	α	1.3	-95.0	12 (63)	1.4E-07
Wild-type	a	23.8		62	
	α	25.9		89	
yor1Δ	a	21.1	-11.3	49	6.6E-02
	α	21.8	-15.8	82	2E-03
Wild-type	a	23.8		55	
	α	20.5		47	
TPO1 (2x)	a	28.9	21.4	42	4E-04
	α	25.5	24.4	58	2E-03
Wild-type	a	26.4		111	
	α	20.5		47	
CTR1 (2x)	a	29.5	11.7	78	3E-02
	α	25.7	25.4	36	9.9E-03
Wild-type	a	26.6		89	
	α	20.5		47	
YOR1 (2x)	a	29.9	12.4	49	4E-03
	α	27.8	35.6	57	5.4E-05

Table S3. Yeast strains constructed and used in this study

Strains	Genotype
BY4741	*MATa; his3Δ0;leu2Δ0;lysΔ0;ura3Δ0*
BY4742	*MATα; his3Δ0;leu2Δ0;lysΔ0;ura3Δ0*
RLY3785	*MATa ; TPO1-GFP::HIS5 his3Δ1;leu2Δ0;met15Δ0;ura3Δ0*
RLY3995	*MATa ; TAT1-GFP::HIS5 his3Δ1;leu2Δ0;met15Δ0;ura3Δ0*
RLY4004	*MATa ; YOR1-GFP::HIS5 his3Δ1;leu2Δ0;met15Δ0;ura3Δ0*
RLY4005	*MATa ; CTR1-GFP::HIS5 his3Δ1;leu2Δ0;met15Δ0;ura3Δ0*
RLY4007	*MATa ; SNQ2-GFP::HIS5 his3Δ1;leu2Δ0;met15Δ0;ura3Δ0*
RLY4008	*MATa ; PDR12-GFP::HIS5 his3Δ1;leu2Δ0;met15Δ0;ura3Δ0*
RLY4085	*MATa; PDR5-GFP::HIS5 GFP-TUB1 CEN URA his3Δ1;leu2Δ0;met15Δ0;ura3Δ0*
RLY4087	*MATa; PDR12-GFP::HIS5 GFP-TUB1 CEN URA his3Δ1;leu2Δ0;met15Δ0;ura3Δ0*
RLY4088	*MATa ; TPO1-GFP::HIS5 GFP-TUB1 CEN URA his3Δ1;leu2Δ0;met15Δ0;ura3Δ0*
RLY4089	*MATa; MRH1-GFP::HIS5 GFP-TUB1 CEN URA his3Δ1;leu2Δ0;met15Δ0;ura3Δ0*
RLY4090	*MATa ; HIP1-GFP::HIS5 GFP-TUB1 CEN URA his3Δ1;leu2Δ0;met15Δ0;ura3Δ0*
RLY4091	*MATa ; SNQ12-GFP::HIS5 GFP-TUB1 CEN URA his3Δ1;leu2Δ0;met15Δ0;ura3Δ0*
RLY4092	*MATa ; HNM1-GFP::HIS5 GFP-TUB1 CEN URA his3Δ1;leu2Δ0;met15Δ0;ura3Δ0*
RLY4093	*MATa ; FUI1-GFP::HIS5 GFP-TUB1 CEN URA his3Δ1;leu2Δ0;met15Δ0;ura3Δ0*
RLY4126	*MATa ; TAT1-GFP::HIS5 GFP-TUB1 CEN URA his3Δ1;leu2Δ0;met15Δ0;ura3Δ0*
RLY4127	*MATa ; CTR1-GFP::HIS5 GFP-TUB1 CEN URA his3Δ1;leu2Δ0;met15Δ0;ura3Δ0*
RLY4128	*MATa ; FET3-GFP::HIS5 GFP-TUB1 CEN URA his3Δ1;leu2Δ0;met15Δ0;ura3Δ0*
RLY4129	*MATa ; VHT1-GFP::HIS5 GFP-TUB1 CEN URA his3Δ1;leu2Δ0;met15Δ0;ura3Δ0*
RLY4130	*MATa ; YOR1-GFP::HIS5 GFP-TUB1 CEN URA his3Δ1;leu2Δ0;met15Δ0;ura3Δ0*
RLY4131	*MATa ; YRO2-GFP::HIS5 GFP-TUB1 CEN URA his3Δ1;leu2Δ0;met15Δ0;ura3Δ0*
RLY4233	*MATα ; TPO1-GFP::HIS5 cdc23-1 ade2;ade3Δ;his3Δ1;leu2-3,112;ura3Δ0;trp1-1*
RLY4234	*MATa ; KAN*::pGAL1-*TPO1-GFP::HIS5 his3Δ1;leu2Δ0;met15Δ0;ura3Δ0*
RLY4235	*MATa ; TPO1-GFP::HIS5 cdc12-6 his3Δ1;leu2Δ0;lys2Δ;ura3Δ0*
RLY4376	*MATa; tpo1Δ::KAN his3Δ0;leu2Δ0;lysΔ0;ura3Δ0*
RLY4378	*MATa; ctr1Δ::KAN his3Δ0;leu2Δ0;lysΔ0;ura3Δ0*
RLY4386	*MATa; yor1Δ::KAN his3Δ0;leu2Δ0;lysΔ0;ura3Δ0*
RLY4840	*MATα; ctr1Δ::KAN his3Δ0;leu2Δ0;lysΔ0;ura3Δ0*
RLY4841	*MATα; yor1Δ::KAN his3Δ0;leu2Δ0;lysΔ0;ura3Δ0*
RLY4842	*MATα; tpo1Δ::KAN his3Δ0;leu2Δ0;lysΔ0;ura3Δ0*
RLY4898	*MATα; 2X TPO1::LEU2 his3Δ0;leu2Δ0;lysΔ0;ura3Δ0*
RLY4899	*MATα; 2X YOR1::LEU2 his3Δ0;leu2Δ0;lysΔ0;ura3Δ0*
RLY4900	*MATα; 2X CTR1::LEU2 his3Δ0;leu2Δ0;lysΔ0;ura3Δ0*
RLY4970	*MATa; 2X TPO1::LEU2 his3Δ0;leu2Δ0;lysΔ0;ura3Δ0*
RLY4971	*MATa; 2X CTR1::LEU2 his3Δ0;leu2Δ0;lysΔ0;ura3Δ0*
RLY4972	*MATa; 2X YOR1::LEU2 his3Δ0;leu2Δ0;lysΔ0;ura3Δ0*
RLY4973	*MATa; TPO1-GFP::HIS5 TPO1-GFP::LEU2 his3Δ0;leu2Δ0;lysΔ0;ura3Δ0*
RLY4981	*MATa; TPO1-GFP::HIS5 mCHERRY-SPC42::LEU2 his3Δ0;leu2Δ0;lysΔ0;ura3Δ0*

All strains used in this study were derivatives of the S288c background.